

# Unified Mie and fractal scattering by cells and experimental study on application in optical characterization of cellular and subcellular structures

Min Xu\*

Fairfield University  
Department of Physics  
1073 North Benson Road  
Fairfield, Connecticut 06824

Tao T. Wu

Jianan Y. Qu\*

Hong Kong University of Science and Technology  
Department of Electronic and Computer  
Engineering  
Clear Water Bay, Kowloon, Hong Kong  
China

**Abstract.** A unified Mie and fractal model for light scattering by biological cells is presented. This model is shown to provide an excellent global agreement with the angular dependent elastic light scattering spectroscopy of cells over the whole visible range (400 to 700 nm) and at all scattering angles (1.1 to 165 deg) investigated. Mie scattering from the bare cell and the nucleus is found to dominate light scattering in the forward directions, whereas the random fluctuation of the background refractive index within the cell, behaving as a fractal random continuous medium, is found to dominate light scattering at other angles. Angularly dependent elastic light scattering spectroscopy aided by the unified Mie and fractal model is demonstrated to be an effective noninvasive approach to characterize biological cells and their internal structures. The acetowhitening effect induced by applying acetic acid on epithelial cells is investigated as an example. The changes in morphology and refractive index of epithelial cells, nuclei, and subcellular structures after the application of acetic acid are successfully probed and quantified using the proposed approach. The unified Mie and fractal model may serve as the foundation for optical detection of precancerous and cancerous changes in biological cells and tissues based on light scattering techniques. © 2008 Society of Photo-Optical Instrumentation Engineers. [DOI: 10.1117/1.2907790]

**Keywords:** Mie scattering; fractal scattering; angularly dependent elastic light scattering spectroscopy; biological cells and tissues; optical biopsy; optical detection of precancerous and cancerous changes in biological cells and tissues.

Paper 07326RR received Aug. 16, 2007; revised manuscript received Nov. 6, 2007; accepted for publication Nov. 7, 2007; published online Apr. 23, 2008; corrected Apr. 29, 2008.

## 1 Introduction

Light interaction with small particles is the foundation for biomedical optical spectroscopy and imaging. Elastic light-scattering spectroscopy (LSS) has been extensively investigated to probe precancerous and cancerous tissue states both *in vivo* and *ex vivo*, and to assess the presence and concentration of biochemicals for diagnostic purposes.<sup>1,2</sup> The optical properties of biological cells and tissues are determined by their microstructures and local refractive index variations. Mammalian cells are typically 10 to 30  $\mu\text{m}$  in diameter. Microstructures in biological tissues and cells range from organelles 0.2 to 0.5  $\mu\text{m}$  or smaller, mitochondria 1 to 4  $\mu\text{m}$  in length and 0.3 to 0.7  $\mu\text{m}$  in diameter, and nuclei 3 to 10  $\mu\text{m}$  in diameter. The refractive index variation is about 0.04 to 0.10 with a background refractive index  $n_0 = 1.35$  for soft tissues.<sup>3</sup> The premise of LSS is that elastic light scattering is sensitive to the morphology of microstructures and the refractive index variations inside cells and tissues and can be used to probe the changes in morphology and refractive index if any (optical biopsy). Due to the complexity of

biological cells, it has been a difficult and challenging task to link the observed light scattering signals to the underlying morphological and refractive index changes inside cells and tissues. The size of scattering centers obtained using Mie models is too small to account for either the cell or the nucleus.<sup>4</sup> The finite difference time domain (FDTD) simulation for light scattering by cells showed the importance of the fluctuation of the refractive index in elastic light scattering by cells,<sup>5</sup> which manifested the deficiency of the Mie model.

It was later observed that the distribution of the refractive index of biological cells and tissues is similar to a fractal. A fractal random fluctuation continuous medium model was found to describe well both the wavelength dependence and angular patterns in larger scattering angles ( $\geq 5$  to 10 deg) of elastic light scattering by biological cells and tissues.<sup>6,7</sup> The well-known power law governing the wavelength dependence of the reduced scattering coefficient of biological samples emerges naturally from such a model. Experimental results, however, demonstrated that light scattering by cells at smaller scattering angles ( $< 5$  deg) retains Mie oscillatory patterns. These oscillatory patterns are attributed to light scattering by

\*Address all correspondence to Min Xu, E-mail: mxu@mail.fairfield.edu; and Jianan Y. Qu, E-mail: eequ@ust.hk.

the whole cell and the embedded nucleus, which dominate in the forward scattering directions. A more realistic model of biological cells shall be a complex composite particle (1) with the nucleus (the most important scattering center in the cell) embedded inside a bare cell host and (2) with the presence of random fluctuation of the background refractive index inside the cell. Such a unified Mie and fractal model has been reported to describe elastic light scattering by biological cells and tissues into both small and large angles for the first time.<sup>8</sup> The unified Mie and fractal model may serve as the foundation for developing optical methods for detecting precancerous and cancerous changes in biological cells and tissues using light scattering techniques.

In this paper, we first present in detail the unified Mie and fractal model introduced in Ref. 8 for elastic light scattering by biological cells and tissues. By comparing the unified model to angularly dependent elastic light scattering spectroscopy for human cervical squamous carcinoma epithelial (SiHa) cells over the spectral range of 400 to 700 nm and the scattering angles of 1.1 to 165 deg, the unified model is shown to provide an excellent global agreement to the experimental data over all scattering angles and all the wavelengths of light investigated. The small-angle light scattering behavior is shown to be determined by the bare cell and the nucleus, whereas the large-angle light scattering behavior is dominated by the fluctuation of the background refractive index within the cell. The changes in morphology and refractive index of epithelial cells, nuclei, and subcellular structures induced by the application of acetic acid on epithelial cells are successfully probed and quantified from the angularly dependent elastic light scattering spectroscopy using the unified Mie and fractal model. Finally, a few outstanding issues about light scattering by biological cells and tissues are addressed.

## 2 Theory

Biological cells have a complex structure. The computation of light scattering property of such particles is usually difficult and time consuming.<sup>9</sup> Techniques such as the FDTD method may be time prohibitive to be used in characterizing biological cells and tissues from light scattering measurements where repeated evaluations of the scattering characteristics of the system prescribed by a set of parameters are required until one set of parameters is found that produce an optimal fitting to the measurements. Mie models are thus commonly used despite their well-known deficiency. Based on one key characteristic of biological cells and tissues that they are optically soft with their refractive index typically varying from ~1.36 for the cytoplasm to ~1.40 for the nucleus, one recent development of the superposition rule for light scattering by soft complex particles<sup>10</sup> provides, for the first time, a tractable approach to analyze the behavior of light scattering by biological cells and tissues.

The light scattering property of spherical or randomly oriented nonspherical particles is characterized by a  $2 \times 2$  diagonal amplitude scattering (Jones) matrix  $\text{diag}(S^{\parallel}, S^{\perp})$  dependent on the particle size parameter, relative refractive index, and the scattering angle, where  $S^{\parallel}$  and  $S^{\perp}$  are the scattering amplitude functions for light of parallel or perpendicular polarization with respect to the scattering plane, respectively.<sup>11,12</sup> The superposition rule<sup>10</sup> shows that the scattering amplitude

function  $S(\mathbf{q})$  (either  $S^{\parallel}$  and  $S^{\perp}$ ) for a composite particle can be approximated by the superposition of the scattering amplitude function  $S_0(\mathbf{q})$  of the host particle and the scattering amplitude functions  $S_i(\mathbf{q})$  of the inclusions:

$$S(\mathbf{q}) = S_0(\mathbf{q}) + \sum_i \exp(-i\mathbf{r}_i \cdot \mathbf{q} - i\bar{\rho}_i)S_i(\mathbf{q}), \quad (1)$$

where  $\mathbf{r}_i$  is the center of the  $i$ 'th inclusion,  $\bar{\rho}_i$  is the average phase delay seen by the  $i$ 'th inclusion due to the shadowing by the host particle,  $\mathbf{q} = q(\cos \phi, \sin \phi, 0)$  is the wave vector transfer with a magnitude  $q = 2k \sin(\theta/2)$ ,  $k = 2\pi n/\lambda$  is the wave number with  $n$  the refractive index of the background medium and  $\lambda$  the wavelength of the incident beam in vacuum, and  $\theta$  and  $\phi$  are the polar and azimuthal angles of scattering, respectively. The superposition rule is valid as long as the maximum difference in the phase delay seen by the inclusions  $(\Delta\rho_i)_{\max} < 1$ . Each shadowed inclusion is the same as the real one except that its refractive index is to be replaced by  $m_i - m_0 + 1$  where  $m_0$  and  $m_i$  are the relative refractive indices of the host and the  $i$ 'th inclusion (compared to the background), respectively. By expressing light scattering by a composite particle as a superposition of light scattering by the host and its inclusions, the superposition rule quantifies the contribution from each individual inclusion embedded in a composite particle and provides a useful means to probe the changes in the internal structure from light scattering by composite particles.

For a typical biological cell of radius  $a \sim 10 \mu\text{m}$  and relative refractive index  $m_0 \sim 1.01$  in aqueous suspensions, the value of the maximum phase delay difference can be estimated to be  $(\Delta\rho)_{\max} \sim 0.4$  for incident light of wavelength 500 nm. Hence, the superposition rule is, in particular, suited to investigate light scattering by biological cells with internal structures (nucleus, mitochondria, and other organelles).

The amplitude scattering function for biological cells is given by the superposition of those of the host (the bare cell), the nucleus, and the random fluctuation of the background refractive index within the cell, i.e.,

$$S_{\text{cell}}(\mathbf{q}) = S_0(\mathbf{q}) + \exp(-i\mathbf{r}_c \cdot \mathbf{q} - i\bar{\rho}_c)S_n(\mathbf{q}) + \sum_i \exp(-i\mathbf{r}_i \cdot \mathbf{q} - i\bar{\rho}_i)S_i(\mathbf{q}). \quad (2)$$

Here the first two terms represent the scattering amplitude function of the bare cell and the nucleus for either parallel or perpendicular polarized light, respectively. The nucleus is centered at  $\mathbf{r}_c$  and sees a phase delay  $\bar{\rho}_c$  due to the shadowing of the host. The third term presents the summation of all contributions from the random fluctuation of the refractive index  $\delta m(\mathbf{r}_i) = m(\mathbf{r}_i) - m_0$  at position  $\mathbf{r}_i$  with a corresponding phase delay  $\bar{\rho}_i$ . The intensity of light scattered into direction  $\mathbf{q}$ , normally measured in the light scattering measurement, is given by the configurational average of the scattering cross section  $|\overline{S_{\text{cell}}(\mathbf{q})}|^2/k^2$  over all possible size, shape, and orientation of the cell and the relative position of its inclusions. The squared scattering amplitude function can be approximated simply by

$$|\overline{S_{\text{cell}}(\mathbf{q})}|^2 = |S_0(\mathbf{q})|^2 + |S_n(\mathbf{q})|^2 + |S_{\text{bg}}(\mathbf{q})|^2, \quad (3)$$

after performing the configuration average, where

$$|S_{\text{bg}}(\mathbf{q})|^2 = 2\pi k^6 V \hat{R}(q) \begin{cases} \mu^2 & \text{parallel polarized} \\ 1 & \text{perpendicular polarized,} \end{cases} \quad (4)$$

is the fractal scattering term (see the Appendix for the proof),  $\mu \equiv \cos \theta$ ,  $V$  is the volume of the cell, and  $\hat{R}(q) = [1/(2\pi)^3] \int R(r) \exp(i\mathbf{q} \cdot \mathbf{r}) d\mathbf{r}$  is the power spectrum of the random fluctuation  $R(|\mathbf{r}_1 - \mathbf{r}_2|) = \langle \delta m(\mathbf{r}_1) \delta m(\mathbf{r}_2) \rangle$  of the background refractive index satisfying  $\langle \delta m(\mathbf{r}) \rangle = 0$ . Among the three terms in Eq. (3), the first two terms from Mie scattering of the bare cell (the uniform cell without any internal structure) and the nucleus dominates forward light scattering by a cell; and the third term from the fluctuation of the background refractive index within the cell dominates light scattering at other angles.

The fractal random continuous medium model has been shown to describe well the random fluctuation of the background refractive index for biological tissues and cells.<sup>6,7</sup> In the fractal model, the random fluctuation of the background refractive index is assumed to be

$$R(r) = \langle \delta m(0)^2 \rangle \int_0^{l_{\max}} \exp\left(-\frac{r}{l}\right) \eta(l) dl, \quad (5)$$

where  $\eta(l) = \eta_0 l^{3-D_f} / l_{\max}^{4-D_f}$  ( $0 \leq l \leq l_{\max}$ ) is the distribution of the correlation length  $l$  normalized to  $\int_0^{l_{\max}} \eta(l) dl = 1$ ,  $\langle \delta m(0)^2 \rangle$  is the squared amplitude fluctuation of the refractive index,  $\eta_0$  is a dimensionless constant, and  $D_f$  is the fractal dimension. The power spectrum of the fluctuation of the refractive index is given explicitly by

$$\hat{R}(k) = \beta^2 \int_0^{l_{\max}} \frac{l^{6-D_f}}{\pi^2 l_{\max}^{4-D_f} (1+k^2 l^2)^2} dl, \quad (6)$$

where  $\beta^2 \equiv \langle \delta m(0)^2 \rangle \eta_0$  is the effective squared amplitude fluctuation of the refractive index. The dimensionless  $\beta$  represents the random fluctuation strength. The background squared scattering amplitude is now

$$|S_{\text{bg}}(\mathbf{q})|^2 = \frac{2}{\pi} \beta^2 V k^{D_f-1} l_{\max}^{D_f-4} \int_0^{k l_{\max}} \frac{x^{6-D_f}}{[1+2(1-\mu)x^2]^2} \times dx \begin{cases} \mu^2 & \text{parallel polarized} \\ 1 & \text{perpendicular polarized.} \end{cases} \quad (7)$$

The intensity of scattered parallel or perpendicular polarized light is proportional to the corresponding scattering cross section given by  $|S_{\text{cell}}(\mathbf{q})|^2 / k^2$  from Eq. (3), where  $|S_0(\mathbf{q})|^2$ ,  $|S_n(\mathbf{q})|^2$ , and  $|S_{\text{bg}}(\mathbf{q})|^2$  are the squared scattering amplitude functions for light of respective polarization. The scattering cross sections for unpolarized light is given by the mean of the two scattering cross section for light of parallel or perpendicular polarization.

To account for the polydispersity of cells, the radius of the bare cell and that of the nucleus are assumed to follow a lognormal distribution:

$$f_i(x) = \frac{1}{\sqrt{2\pi}\delta_i} x^{-1} \exp\left[-\ln^2\left(\frac{x}{a_{m_i}}\right) / 2\delta_i^2\right], \quad (8)$$

with  $i=0$  standing for the bare cell, and  $i=1$  for the nucleus, respectively. The lognormal size distribution of parameters  $a_m$  and  $\delta$  attains its peak at  $a_m / \exp(\delta^2)$  and a full width at half maximum (FWHM) of the size distribution to be  $2 \sinh(\sqrt{2 \ln 2} \delta) a_m / \exp(\delta^2)$ . The average volume is given by  $V = (4/3)\pi a_m^3 \exp[(9/2)\delta^2]$ . The two important characteristics of the size distribution are the effective radius

$$a^{\text{eff}} = \frac{\int_0^\infty x^3 f(x) dx}{\int_0^\infty x^2 f(x) dx} = a_m \exp(5\sigma^2/2) \quad (9)$$

and the effective variance

$$\nu^{\text{eff}} = \frac{\int_0^\infty (x - a^{\text{eff}})^2 x^2 f(x) dx}{(a^{\text{eff}})^2 \int_0^\infty x^2 f(x) dx} = \exp(\sigma^2) - 1. \quad (10)$$

These two characteristics are geometrical projection area weighted. Scatterers of different size distributions but of the same effective radius and effective variance behave alike in their properties of light scattering.<sup>9</sup> These two parameters are reported in the fitting results.

In our analysis presented in the following sections, the first two terms in Eq. (3) are computed using a regular Mie scattering code weighted by the lognormal size distribution.<sup>13</sup> The third term in Eq. (3) is evaluated by a numerical integration of Eq. (7). The measured angular spectra of light scattering versus the scattering angle  $\theta$  and the wavelength  $\lambda$  are then used to extract the size distribution ( $a_{m_0}$  and  $\delta_0$ ) and the relative refractive index  $m_0$  of the bare cell, the size distribution ( $a_{m_1}$  and  $\delta_1$ ) and the relative refractive index  $m_1$  of the nucleus, and the fractal dimension  $D_f$ , the cutoff correlation length  $l_{\max}$ , and the fluctuation strength  $\beta$  of the background refractive index fluctuation.

### 3 Results

In this section, the unified model presented in Eq. (3) is used to analyze angular dependent light scattering spectroscopy for human cervical squamous carcinoma epithelial (SiHa) cells over the spectral range 400 to 700 nm and the scattering angles from 1.1 to 165 deg. The details of the experimental setup were given elsewhere.<sup>14</sup> The size distribution of the SiHa cells in phosphate buffered saline (PBS) suspensions was measured by phase contrast microscopy and verified by a Multisizer II Coulter counter. The size distribution of nuclei was measured by fluorescence microscopy. The nuclei were stained with Hoechst 33342 for fluorescence microscopic imaging. The size distributions of SiHa cells and nuclei were described by log-normal distributions, as in Eq. (8). Specifically, the radii of the cells in suspension before and after the application of acetic acid were  $a_{m_0} = 6.85 \mu\text{m}$  and  $\delta_0 = 0.116$  and  $a'_{m_0} = 7.14 \mu\text{m}$  and  $\delta'_0 = 0.125$ , respectively. The radii of

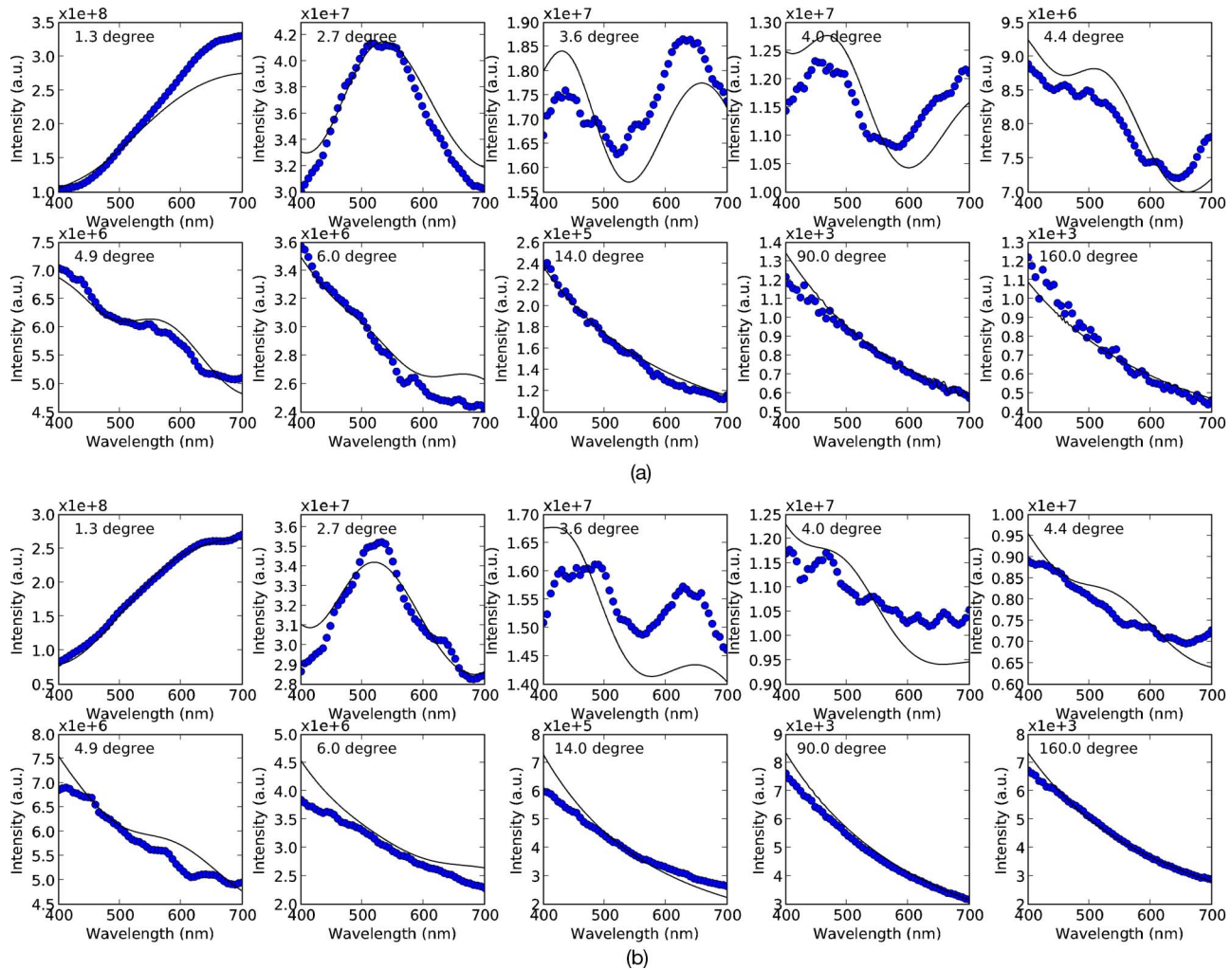


**Fig. 1** Experimental (solid circles) and unified model fitting (solid line) results for the scattering spectra of the SiHa cell suspension before and after the application of acetic acid at 10 representative scattering angles. The size distributions for the cell and the nucleus were measured separately by microscopy and not fitted.

nuclei before and after the application of acetic acid were  $a_{m_1}=4.82 \mu\text{m}$  and  $\delta_1=0.182$ , and  $a'_{m_1}=4.58 \mu\text{m}$  and  $\delta'_1=0.171$ , respectively. These size distributions were used in fitting of the scattering spectral data. The refractive index of the PBS and the acetic acid solution was assumed to be 1.334.

A global fitting for the light scattering spectra over 400 to 700 nm at a total of 44 scattering angles ranging from 1.1 to 165 deg was conducted by minimizing the chi-squared error of logarithm intensities using a Levenberg-Marquardt algorithm. The fitting parameters were the refractive indices of the cell and the nucleus ( $m_0$  and  $m_1$ ), the fractal dimension  $D_f$ , the refractive index fluctuation strength  $\beta$ , and the cutoff correlation length  $l_{\text{max}}$ . Initial values for the refractive indices  $m_0$  and  $m_1$  were obtained by fitting the scattering spectra in the angular range smaller than 5 deg. Initial values for  $D_f$  and  $l_{\text{max}}$  were obtained by fitting the scattering spectra in the angular range larger than 20 deg.

Figure 1 displays the representative fitting results for 10 scattering angles before and after the application of acetic acid to the SiHa cell suspension. The fitting parameters are summarized in Table 1.

In a second attempt to fit the experimental data to investigate whether the angularly dependent light scattering spectroscopy alone can be used to characterize the biological cell, the size distributions of the bare cell and the nucleus were assumed to be unknown. In this case, the initial values for the bare cell ( $a_{m_0}$ ,  $\delta_0$ , and  $m_0$ ) were fitted from the wavelength-dependent light intensities scattered into angles less than 2 deg (total five angles of 1.1, 1.3, 1.6, 1.8, and 2.0 deg), where light scattering is dominated by the bare cell. The initial values for the nucleus were assumed to be  $a_{m_1}=2a_{m_0}/3$ ,  $\delta_1=\delta_0$ , and  $m_1=1.06$ . These values for the bare cell and the nucleus were then updated by fitting the wavelength-dependent light intensities scattered into angles less than 4 deg (total 15 angles of 1.1, 1.3, 1.6, 1.8, 2.0, 2.2, 2.4, 2.7, 2.9, 3.1, 3.3, 3.6, 3.8, and 4.0 deg), where light scattering is dominated by the bare cell and the nucleus together. Initial values for  $D_f$  and  $l_{\text{max}}$  were obtained by fitting the scattering spectra in the angular range larger than 20 deg. The initial value for the background refractive index fluctuation was set to  $\beta=0.01$ . A global fitting for the light scattering spectra over 400 to 700 nm at total 44 scattering angles was then

**Table 1** Fitting parameters for the SiHa cell suspension before and after the application of acetic acid (AA).

	$\alpha_{\text{cell}}^{\text{eff}}$ ( $\mu\text{m}$ )	$\nu_{\text{cell}}^{\text{eff}}$	$\alpha_{\text{nucleus}}^{\text{eff}}$ ( $\mu\text{m}$ )	$\nu_{\text{nucleus}}^{\text{eff}}$	$n_{\text{cell}}$	$n_{\text{nucleus}}$	$D_f$	$l_{\text{max}}$ ( $\mu\text{m}$ )	$\beta$	Error
Before AA	7.08	0.0135	5.24	0.0337	1.367	1.393	4.48	0.413	0.0089	4.55
After AA	7.42	0.0157	4.93	0.0297	1.360	1.405	4.68	0.340	0.0194	3.20

The size distributions for the cell and the nucleus ( $\alpha_{\text{cell}}^{\text{eff}}$ ,  $\nu_{\text{cell}}^{\text{eff}}$ ,  $\alpha_{\text{nucleus}}^{\text{eff}}$  and  $\nu_{\text{nucleus}}^{\text{eff}}$ ) were measured separately by microscopy and not fitted. The refractive indices ( $n_{\text{cell}}$  and  $n_{\text{nucleus}}$ ) and the parameters for the background refractive index fluctuation ( $D_f$ ,  $l_{\text{max}}$ , and  $\beta$ ) were obtained by fitting all scattering spectra at 44 scattering angles using the unified Mie and fractal model.

conducted by minimizing the chi-squared error of logarithm intensities.

Figure 2 displays the representative fitting results for the same 10 scattering angles before and after the application of acetic acid to the SiHa cell suspension. The fitting parameters are summarized in Table 2. The parameters are very close to the values obtained in the first fitting, where the size distributions of the cell and the nucleus were measured separately by microscopy and not fitted. In particular, the recovered size

distributions of the cells and the nuclei agree with the independent measurements by microscopy.

The fitting to angularly dependent scattering spectroscopies is much more stringent than that to the scattering spectrum at a specific wavelength of light. The fitting results already obtained from fitting to the former yields almost perfect agreement to the scattering spectrum at any one particular wavelength. Figure 3 demonstrates such an agreement for in-

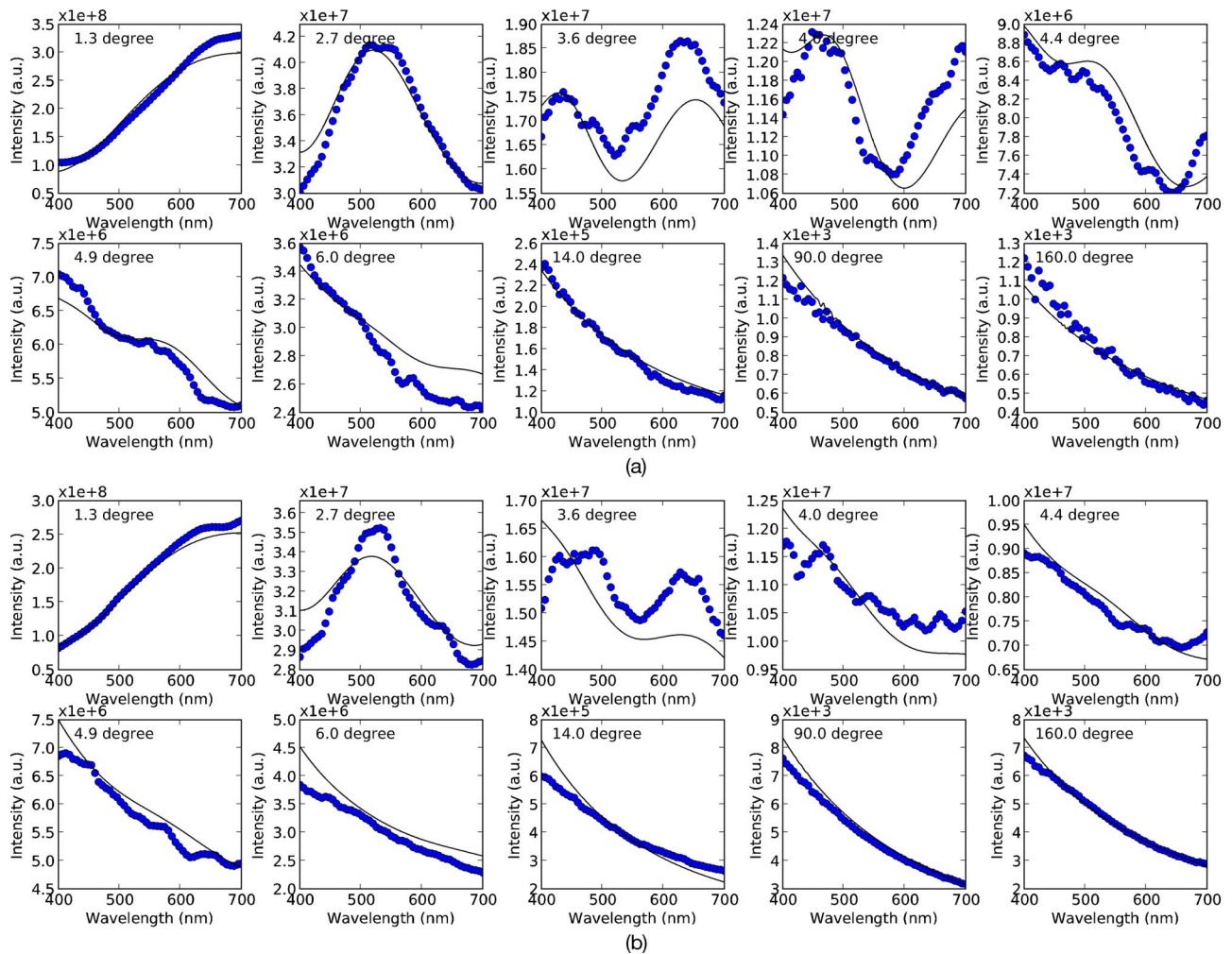


**Fig. 2** Experimental (solid circles) and unified model fitting (solid line) results for the scattering spectra of the SiHa cell suspension before and after the application of acetic acid at 10 representative scattering angles. The size distributions of the bare cell and the nucleus were assumed unknown and fitted.

**Table 2** Fitting parameters for the SiHa cell suspension before and after the application of AA using the angularly dependent light scattering spectroscopy alone.

	$\alpha_{\text{cell}}^{\text{eff}}$ ( $\mu\text{m}$ )	$\nu_{\text{cell}}^{\text{eff}}$	$\alpha_{\text{nucleus}}^{\text{eff}}$ ( $\mu\text{m}$ )	$\nu_{\text{nucleus}}^{\text{eff}}$	$n_{\text{cell}}$	$n_{\text{nucleus}}$	$D_f$	$l_{\text{max}}$ ( $\mu\text{m}$ )	$\beta$	Error
Before AA	7.33	0.0137	5.83	0.0776	1.360	1.400	4.45	0.348	0.0093	3.88
After AA	7.39	0.0227	5.08	0.0547	1.360	1.405	4.68	0.337	0.0193	2.86

The size distributions for the cell and the nucleus were fitted together with other parameters. The fitting procedure is detailed in the text.

cident light of wavelength 633 nm. The parameters used in the unified model are the same ones given in Table 2.

The mechanism for the acetowhitening effect,<sup>15</sup> on which colposcopic diagnosis of cervical cancer is based, is clearly illustrated in the changes of the size and the refractive index of the SiHa cell induced by the application of AA from the preceding analysis. After the application of AA, the cell swells and the mean refractive index of the cell decreases slightly. On the contrary, the nucleus shrinks and the mean refractive index of the nucleus increases slightly. The slight increase of the fractal dimension  $D_f$  after the application of AA indicates an increase of the volume fraction of the smaller subcellular structures. The most striking change induced by the application of AA is the doubling of the random fluctuation of the background refractive index. The increase of the refractive index fluctuation amplitude  $\beta$  is  $\sim 2.2$  times after the application of AA. The observed significant enhancement by a factor of 5 to 9 of the large-angle light scattering signal after the application of AA originates from the increased fractal scattering by the cell owing to the stronger background refractive index fluctuation (about 4.8 times larger in  $\beta^2$ ) and the shifting of the size of subcellular structures toward smaller sizes ( $D_f$  increases and  $l_{\text{max}}$  decreases). These findings are consistent with earlier reports and support the hypothesis of acetowhitening effect that AA increases the polymerization of cytokeratins and causes the self-organization of keratin filaments into larger bundles.<sup>14,16</sup>

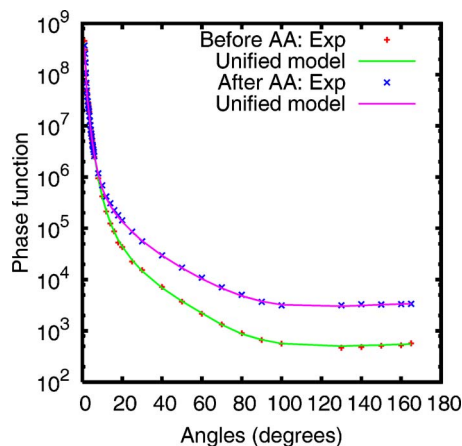


**Fig. 3** Experimental scattering spectra of SiHa cells before and after the application of AA. The wavelength of light is 633 nm. The parameters for the unified model used are given in Table 2.

## 4 Discussion and Conclusion

The significance of this unified Mie and fractal model for light scattering by biological cells is its excellent agreement to the angularly dependent light scattering spectroscopy of biological cells across all scattering angles from forward to backward directions and over the whole spectral range investigated. Most importantly, the agreement between the model and the experimental data when the size distributions of the cells and the nuclei are fixed by independent microscopy measurements demonstrates the validity of the unified model. The recovered refractive indices ( $n_{\text{cell}}=1.360$  to 1.367 and  $n_{\text{nucleus}}=1.393$  to 1.400) for SiHa cells before the application of AA are consistent with earlier findings.<sup>4,17</sup> The changes in morphology and refractive index of epithelial cells, nuclei, and subcellular structures induced by the application of AA on SiHa cells have been successfully quantified from the angularly dependent elastic light scattering spectroscopy using the unified model with or without the knowledge of the size distributions of the cells and the nuclei. This suggests the unified Mie and fractal model may be used to characterize minute changes in the morphology and refractive index of the cell and its internal structure and may serve as the foundation for optical detection of precancerous and cancerous changes in biological cells and tissues based on light scattering techniques. A few outstanding issues concerning light scattering by biological cells and tissues are discussed from the perspective of this unified model.

The angularly dependent contributions of different components to the cell light scattering are displayed in Fig. 4. The largest contribution to the scattered light into scattering angles less than 3.9 deg is that from the bare cell. The largest contribution to light scattering into angles larger than 13.0 deg is from the random fluctuation of the background refractive index. The contribution due to the nucleus is larger than that from the bare cell for scattering angles larger than 5.0 deg. Note that the importance of the components for different cells may differ. Overall, Mie scattering from the bare cell and the nucleus dominates cell light scattering in the forward directions, whereas the random fluctuation of the background refractive index within the cell dominates light scattering by cells in other angles.

The wavelength-dependent behavior of the contributions of different components to the total scattering cross section are displayed in Fig. 5. The bare cell dominates the contribution to light scattering and the refractive index fluctuation contributes least. However, the contribution due to the refractive index fluctuation is significantly enhanced after the application of AA. The contribution due to the refractive index

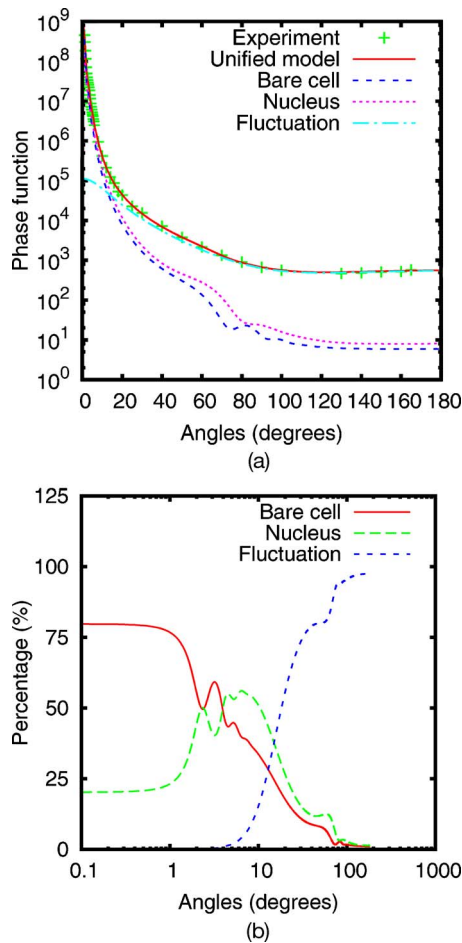


**Fig. 4** Angularly dependent contributions to the scattered light by different components: the bare cell, the nucleus, and the random fluctuation in the background refractive index inside SiHa cells before the application of AA: (a) contributions of each component and (b) percentage of each component in the light scattering signal. The wavelength of light is 633 nm. The contributions to the scattered light by different components after the application of AA are similar and not displayed.

fluctuation is larger than that from the nuclei at shorter wavelengths after the application of AA.

In optical imaging of biological samples, multiple scattering of light inside the sample cannot be avoided. Two important characteristics of the sample are the reduced scattering coefficient  $\mu'_s$  and the anisotropy factor  $g$  (mean cosine of light scattering). The unnormalized  $\mu'_s$  is given by  $\int(1 - \cos \theta) |S_{\text{cell}}(\theta)|^2 / k^2 d \cos \theta \approx \int(1 - \cos \theta) |S_{\text{bg}}(\mathbf{q})|^2 / k^2 d \cos \theta$  and depends mainly on the random fluctuation of the background refractive index. The Mie scattering component concentrates in the forward angles and is much suppressed by the  $(1 - \cos \theta)$  factor. This is the reason why the fractal random continuous medium model works well for biological tissues and cells in optical imaging.<sup>6</sup> This is also the origin of the power law relation  $\mu'_s(\lambda) \propto \lambda^{-\text{SP}}$  ( $\text{SP} = D_f - 3$ ) of the reduced scattering on the wavelength of the probing light despite the presence of Mie scattering in single light scattering by cells. Figure 6 displays the contributions to  $\mu'_s$  by Mie (bare cell and nucleus) and fractal scattering (fluctuation) and the fitting

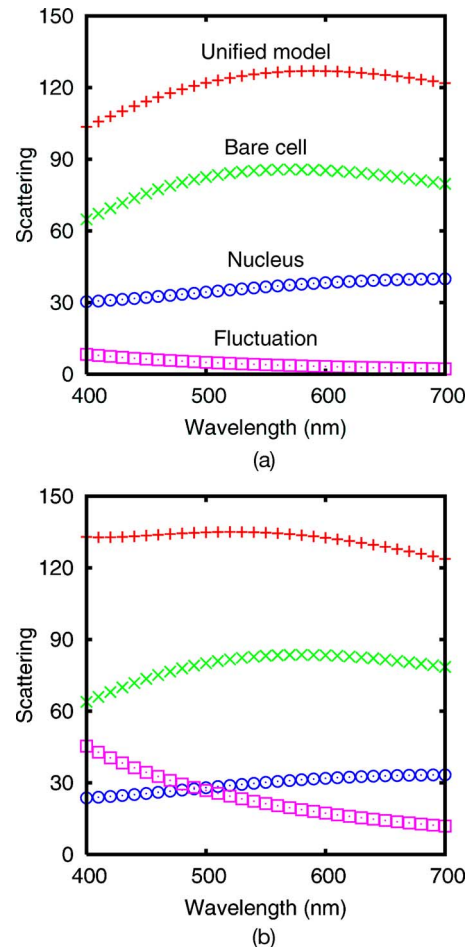


**Fig. 5** Wavelength-dependent contributions to the scattered light by different components: the bare cell, the nucleus, and the random fluctuation in the background refractive index inside SiHa cells (a) before and (b) after the application of AA.

of the power law of  $\mu'_s$  before and after the application of AA. Fractal scattering dominates reduced light scattering. The fitting to the power law of  $\mu'_s$  yields a scattering power of 1.36 and 1.76, respectively. This corresponds to fractal dimensions of 4.36 and 4.76 before and after the application of AA. These values of  $D_f$  deviate slightly from those recovered from the more rigorous analysis presented in Tables 1 and 2. Moreover, fractal scattering is significantly enhanced by application of AA on SiHa cells. This is the reason why the anisotropy factor of SiHa cells decreases appreciably after the application of AA (see Fig. 7).

From the preceding analysis of the relative importance of different components to cell light scattering, we can make the following observations. First, multiple scattering light is sensitive to the refractive index fluctuation inside a biological sample and insensitive to the size or the mean refractive index of the bare cell and the nuclei since the propagation of multiply scattered light in the sample is mainly determined by reduced light scattering  $\mu'_s$  which is dominated by fractal scattering. Attributing reduced light scattering by biological samples to Mie scattering and determining the nuclear size from  $\mu'_s(\lambda)$  is inappropriate. To probe the nuclear size change

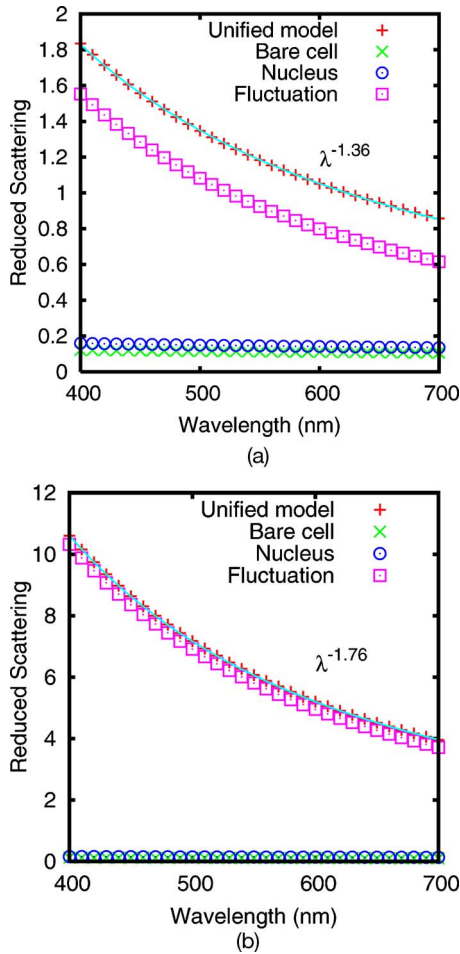


**Fig. 6** Unnormalized reduced scattering of SiHa cells (a) before and (b) after the application of AA. The fitting to the power law of  $\mu_s'$  yields scattering powers of 1.36 and 1.76, respectively, for (a) and (b). The contributions from the bare cell, the nucleus, and the random fluctuation in the background refractive index inside SiHa cells to reduced light scattering are also plotted.

owing to, for example, carcinogenesis, one must acquire additional information about the light scattering property of the sample, such as its anisotropy factor,<sup>18</sup> if multiply scattered light is used. The optical signal from few scattered photons may also be measured for such a purpose by detecting back-scattered light close to the incident source. Even in such an arrangement, few scattered photons are usually buried in a multitude of photons that have undergone multiple scattering because light scattering by biological samples is highly forward peaked ( $g > 0.9$ ). A model taking into consideration multiple scattering of light is still mandatory to interpret such light signals correctly. For either multiply or few scattered light, the unified Mie and fractal model provides the much needed foundation on which a rigorous analysis can be based.

## 5 Appendix

In this appendix, we will prove Eq. (4). Consider a particle with two point scatterers randomly placed inside. According to the superposition rule, the scattering amplitude of the par-

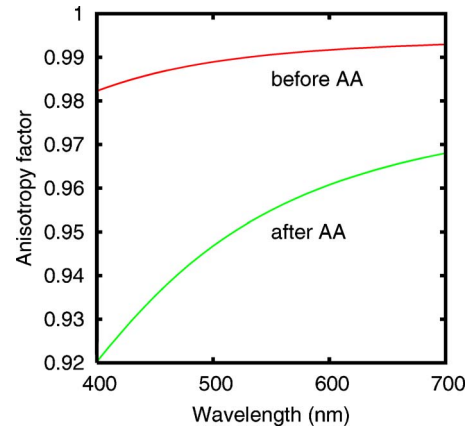


**Fig. 7** Decrease of the anisotropy factor of SiHa cells after the application of AA.

ticle with two point scatterers embedded at  $\mathbf{r}_{1,2}$  can be written as

$$S(\mathbf{q}) = S_0(\mathbf{q}) + \exp(-i\mathbf{r}_1 \cdot \mathbf{q} - i\rho_1)S_1(\mathbf{q}) + \exp(-i\mathbf{r}_2 \cdot \mathbf{q} - i\rho_2)S_2(\mathbf{q}), \quad (11)$$

where  $S_0(\mathbf{q})$  and  $S_{1,2}(\mathbf{q})$  are the scattering amplitude of the bare host particle and the point scatterers, respectively, and  $\rho_{1,2}$  are the phase delay seen by the point scatterers due to the host particle. The phase delay  $\rho_j$  is simply given by  $\rho_{\max}[1 - (\xi_j^2 + \eta_j^2)/a^2]^{1/2}$ , where  $\rho_{\max} \equiv 2k(m_0 - 1)a$  is the maximum phase delay for a ray passing through the host particle whose refractive index is  $m_0$  and whose radius is  $a$ ,  $\xi_j$  and  $\eta_j$  are the  $x$  and  $y$  components of  $\mathbf{r}_j$ , and  $k$  is the wave number of the incident beam in the  $z$  direction. The two point scatterers have an identical volume  $v \ll 1$  and a refractive index  $m_0 + \delta m(\mathbf{r}_j)$ . The amplitude scattering function  $S_j$  for the two point scatterers  $j=1, 2$  is given by

$$S_j(\mathbf{q}) = -\frac{ik^3v}{2\pi}\delta m(\mathbf{r}_j), \quad (12)$$

following Rayleigh-Gans scattering.

Let us now assume the mean of the refractive index fluctuation  $\langle \delta m(\mathbf{r}_j) \rangle = 0$  and the correlation between the two point scatterers  $R(r) \equiv \langle \delta m(\mathbf{r}_1)\delta m(\mathbf{r}_2) \rangle$ , where  $r = |\mathbf{r}_1 - \mathbf{r}_2|$ . The squared scattering amplitude of the composite particle with such two point scatterers randomly placed inside is given by

$$\overline{|S(\mathbf{q})|^2} = |S_0(\mathbf{q})|^2 + 2\left(\frac{k^3v}{2\pi}\right)^2 R(0) + 4\pi(k^3v)^2 V^{-1}\hat{R}(q), \quad (13)$$

where  $V$  is the volume of the host particle, and  $\hat{R}$  is the power spectrum of  $R(r)$  provided that the correlation decays fast enough that a typical separation between the two point scatterers  $r \ll a$ .

The corresponding squared scattering amplitude is given by

$$\begin{aligned} \overline{|S(\mathbf{q})|^2} &= |S_0(\mathbf{q})|^2 + N \left( \frac{k^3 v}{2\pi} \right)^2 R(0) \\ &+ 4\pi \frac{N(N-1)}{2} (k^3 v)^2 V^{-1} \hat{R}(q) \end{aligned} \quad (14)$$

for  $N$  point scatterers. In the limit of  $N \rightarrow \infty$  and  $v \rightarrow 0$  while keeping the product  $Nv = T_v V$  fixed, where  $T_v$  is the dimensionless total volume fraction of point scatterers, we find

$$\overline{|S(\mathbf{q})|^2} = |S_0(\mathbf{q})|^2 + 2\pi T_v^2 k^6 V \hat{R}(q) \quad (15)$$

for the composite particle. In particular,  $\overline{|S(\mathbf{q})|^2} = |S_0(\mathbf{q})|^2 + 2\pi k^6 V \hat{R}(q)$  if  $T_v = 1$ .

### Acknowledgments

MX acknowledges Research Corporation and Fairfield University for their support. JYQ acknowledges the support by the Hong Kong Research Grants Council through Grant No. HKUST6408/05M.

### References

1. J. R. Mourant, J. P. Freyer, A. H. Hielscher, A. A. Eick, D. Shen, and T. M. Johnson, "Mechanisms of light scattering from biological cells relevant to noninvasive optical-tissue diagnostics," *Appl. Opt.* **37**, 3586–3593 (1998).
2. A. Wax, C. Yang, V. Backman, K. Badizadegan, C. W. Boone, R. R. Dasari, and M. S. Feld, "Cellular organization and substructure measured using angle-resolved low-coherence interferometry," *Biophys. J.* **82**, 2256–2264 (2002).
3. J. M. Schmitt and G. Kumar, "Optical scattering properties of soft tissue: a discrete particle model," *Appl. Opt.* **37**, 2788–2797 (1998).
4. J. R. Mourant, T. M. Johnson, S. Carpenter, A. Guerra, T. Aida, and J. P. Freyer, "Polarized angular dependent spectroscopy of epithelial cells and epithelial cell nuclei to determine the size scale of scattering structures," *J. Biomed. Opt.* **7**, 378–387 (2002).
5. D. Arifler, M. Guillaud, A. Carraro, A. Malpica, M. Follen, and R. Richards-Kortum, "Light scattering from normal and dysplastic cer-

- vical cells at different epithelial depths: finite-difference time-domain modeling with a perfectly matched layer boundary condition," *J. Biomed. Opt.* **8**, 484–494 (2003).
6. M. Xu and R. R. Alfano, "Fractal mechanisms of light scattering in biological tissue and cells," *Opt. Lett.* **30**, 3051–3053 (2005).
7. M. Xu, M. Alrubaiee, and R. R. Alfano, "Fractal mechanism of light scattering for tissue optical biopsy," in *Optical Biopsy VI, Proc. SPIE 6091*, 60910E (2006).
8. T. T. Wu, J. Y. Qu, and M. Xu, "Unified Mie and fractal scattering by biological cells and subcellular structures," *Opt. Lett.* **32**, 2324–2326 (2007).
9. M. I. Mishchenko, L. D. Travis, and A. A. Lacis, *Scattering, Absorption and Emission of Light by Small Particles*, Cambridge University Press, Cambridge (2002).
10. M. Xu, "Superposition rule for light scattering by a composite particle," *Opt. Lett.* **31**, 3223–3225 (2006).
11. H. C. van de Hulst, *Light Scattering by Small Particles*, Dover, New York (1981).
12. R. C. Jones, "A new calculus for the treatment of optical system: I description and discussion of the calculus," *J. Opt. Soc. Am.* **31**, 488–493 (1941).
13. W. J. Wiscombe, "Improved Mie scattering algorithms," *Appl. Opt.* **19**, 1505–1509 (1980).
14. T. T. Wu and J. Y. Qu, "Assessment of the relative contribution of cellular components to the acetowhitening effect in cell cultures and suspensions using elastic light-scattering spectroscopy," *Appl. Opt.* **21**, 4834–4842 (2007).
15. M. C. Anderson, J. A. Jordan, A. R. Morse, and F. Sharp, *A Text and Atlas of Integrated Colposcopy for Colposcopists, Histopathologists, and Cytologists*, Chapman & Hall Medical, London (1992).
16. R. Lambert, J. F. Rey, and R. Sankaranarayanan, "Magnification and chromoscopy with the acetic acid test," *Endoscopy* **35**, 437–445 (2003).
17. R. Drezek, A. Dunn, and R. Richards-Kortum, "A pulsed finite-difference time-domain (FDTD) method for calculating light scattering from biological cells over broad wavelength ranges," *Opt. Express* **6**, 147–157 (2000).
18. M. Xu, M. Alrubaiee, S. K. Gayen, and R. R. Alfano, "Determination of light absorption, scattering and anisotropy factor of a highly scattering medium using backscattered circularly polarized light," in *Optical Interactions with Tissue and Cells XVIII, Proc. SPIE 6435*, 64350J (2007).